Solid State Sciences 128 (2022) 106885

Contents lists available at ScienceDirect

Solid State Sciences

journal homepage: www.elsevier.com/locate/ssscie

Solvent directs the dimensionality of Cu-dicyanoimidazoles

Pipsa Hirva [a,*], Sirpa Jääskeläinen [a], Rezeda Gayfullina [b], Henna Korhonen [a], Igor O. Koshevoy [a]

[a] Department of Chemistry, University of Eastern Finland, P.O. Box 111, Fi-80101, Joensuu, Finland
[b] Department of Chemistry, University of Jyväskylä, P.O. Box 35, FI-40014, Jyväskylä, Finland

ARTICLE INFO

Keywords:
Copper complex
Imidazole
Cyano
Solvent effect
DFT
QTAIM

ABSTRACT

In this paper, we report one-pot reactions of the same reactants 4,5-dicyanoimidazole and CuI in different solvents. In pure MeCN, the reaction resulted in previously reported MOF structure $[Cu(4,5\text{-dicyanoimidazole})]_n(MeCN)_{0.5n}$ (**1**). On the other hand, when MeCN/MeOH solvent mixture was used, a new coordination polymer $[Cu(4,5\text{-dicyanoimidazole})(MeCN)(CuI)]_n$ (**2**) was formed. The crystallization yielded very different structures as determined by X-ray crystallography. In **1**, the solvent molecule acetonitrile occupies the MOF pores *via* weak interactions, but in **2** it is coordinated to the metal center. Computational DFT calculations and topological charge density analysis were utilized to explore the different crystal structures with the focus on the role of the methanol solvent.

1. Introduction

Porous metal organic frameworks, MOF structures, are at the moment one of the main areas in coordination chemistry, with the focus on the synthesis of these fascinating architectures and the tunability of the structures to obtain desired characteristics. Creditable reviews about the manifold syntheses and the effect of reaction conditions on the framework architectures [1–5] as well as their applications e.g. in energy storage [6,7], gas storage [8], electrochemical materials [9], luminescent materials [10], catalysis [11], and magnetic materials [12,13] are available, including also studies of the bio-significance of chiral MOFs [14].

The aim in the MOF studies is mainly focused on directing the synthesis to obtain desired architectures and hence desired functionality in applications. There are lots of challenges since the reaction conditions have crucial impact on the self-assembly. The combination of reaction variables e.g. the precursor choice [15,16], the reaction type [17,18], the solvent [19], the pH [20], the temperature [21], the molar ratios [22], the concentrations [23], the counter-ions [24] and manipulation of crystal growth, guide the reactions. However, there seems to be no governing rules for the effect, but the ample studies rather give the parameters for specific metal/ligand systems [25]. For example, the effect of the solvent has been explained by the terms of solubility, solvation, hydrogen bonding [26], coordination ability, molecular size, effect on pH, effect on the protonation/deprotonation process, polarizability, or kinetics of the crystal growth process [27]. It still seems to be a great challenge to construct the preferred structures.

Very often the systems contain nitrogen ligands, such as aromatic pyridines, pyrimidines, imidazoles, or cyanides. One ligand with potentiality to MOF structures is 4,5-dicyanoimidazole. In 2016, Hu et al. reported the synthesis and crystallographic studies on $[Cu(4,5\text{-dicyanoimidazole})]_n(0.1cyclohexanol,0.45nitrobenzene)_n$ [28], formed in the solvothermal synthesis. The Cu(I)-dicyanoimidazole MOF with solvent in pores was found to crystallize in chiral space group. The adsorption/desorption properties of the material were reported. Further, the CD spectrum was measured to characterize the optical activity and the photoluminescent behavior. In 2017, Zhao et al. prepared in a large scale at room temperature the corresponding MOF with MeCN in the pores [29]. The structure shows exceptional resistance towards many chemicals, offering great potentiality to practical use. In both articles, TGA was used to examine the solvent amount in pores.

Furthermore, a selection of organic amines has been utilized as templates to create MOF structures with 4,5-dicyanoimidazole. The protonated amines were suggested to have an important role in templating the structure and were located at the cavities. The one-pot syntheses in the presence of CuI created frameworks based on Cu_4I_4 clusters bridged by tetradentate dicyanoimidazoles [30].

In this work, we prepared derivatives of 4,5-dicyanoimidazole with CuI in constant reaction conditions except for the solvent in crystallization. In addition to experimental studies, the effect of the solvent was computationally studied to explain its role in the formation of the crystalline structures.

* Corresponding author.
E-mail address: pipsa.hirva@uef.fi (P. Hirva).

https://doi.org/10.1016/j.solidstatesciences.2022.106885
Received 22 October 2021; Received in revised form 28 February 2022; Accepted 11 April 2022
Available online 14 April 2022

2. Results and discussion

2.1. Syntheses and characterization

In this work, we carried out the room temperature, one-pot syntheses between CuI and 4,5-cyanoimidazole. If pure acetonitrile was used in crystallization, colorless cubic crystals of $[Cu(4,5\text{-dicyanoimidazole})]_n(MeCN)_{0.5n}$ (1) with MeCN molecules in the pores was formed (Fig. 1). The crystallographic study confirmed the structure consistent with the one published by Zhao [29]. The space group was $I4_122$ in both determinations. The cell axes were a 9.2513(8) Å, b 9.2513(8) Å, c 22.2791(19) Å whereas the values for Zhao's determination were a 9.281(17) Å, b 9.281(17) Å, c 22.07(5) Å. The temperature in our measurement was 150 K, in Zhao's work it was 293 K. The data collection was done using Mo K_α radiation ($\lambda = 0.71073$ Å) in both cases. The ligand is deprotonated and acts as a four-electron donor. Thus, each nitrogen is bonded to copper centers.

When the solvent was changed to MeCN/MeOH mixture, a new polymeric compound $[Cu(4,5\text{-dicyanoimidazole})(MeCN)(CuI)]_n$ (2) as light yellow needle-like crystals was obtained (Fig. 2). The crystallographic data is given in supporting information. The compound crystallizes in non-centrosymmetric space group $P2_1/c$. In this case, the MeCN solvent molecule is coordinated through the cyano group to the metal center. The environment of each copper center is a trigonal plane, in which two deprotonated imidazole groups are accompanied by an acetonitrile molecule. The -Cu(acetonitrile)L-chains are connected to Cu_2I_2 units through one of the cyano groups of the ligands. The other cyano group remains unattached, but connects to the neighboring ligands or solvent *via* weak hydrogen-bonding interactions. The strength of the H-bonding interactions was −5 to −6 kJ/mol, according to the QTAIM (Quantum Theory of Atoms in Molecules) analysis. The Cu–Cu distance is 3.273 Å between the layers.

Both syntheses were repeated several times with various concentrations and molar ratios, but always the same products were obtained. Therefore, we can conclude that only the presence of MeOH controls the course of the reaction. The role of MeOH as structure directing agent might be thought to be a solubility factor. Thus, if the solubility of CuI is diminished in the presence of the alcohol, this could cause its easier involvement in the crystallization and the final product. The presence of MeOH enhances the coordination of MeCN molecule. Calculations of the electron density revealed, that in MeOH solvent field the negative charge of the nitrogen of the MeCN increases, thus facilitating its coordination into a metal cation (Table 1). The steric hindrance of the solvent molecule has also been suggested to control the reaction, but obviously the steric hindrance between CH_3CN/CH_3OH is not crucial.

The experimental IR spectra of the crystalline products in KBr showed the major ν(C–N) peak at 2233 cm^{-1} for **1**, 2245 and 2233 cm^{-1} for **2**, while the values for free ligand are 2261 and 2246 cm^{-1}. The shift to lower frequencies is usually associated to the side-on coordination of the cyano group. The shifts to higher frequencies are usually attributed to the end-on coordination of nitrile to the metal center, but systematic information that links the coordination mode and the shift is lacking [31]. In order to explain the shifts observed in the experimental spectra, we simulated the IR spectra at the DFT level. However, to get reliable IR frequencies, the structures of the molecular models must be optimized. Therefore, we created small molecular models from the initial crystal structures including only the closest coordination sphere of copper ions. It was also necessary to terminate the models with additional hydrogen atoms attached to the imidazole nitrogens to mimic copper coordination to surrounding units and to ensure optimized geometries as close to the crystal structures as possible. The optimized models $[Cu(4,5\text{-dicyanoimidazole})_4]$ and $[Cu(4,5\text{-dicyanoimidazole})_2(MeCN)]$ (M1 and M2, respectively) are presented in Figure S1 and the corresponding simulated IR spectra are shown in Figure S2. Although the models represent the coordination sphere of each copper atoms well, they cannot account for longer range symmetry of the crystal structures. For example, in M1 there are both coordinated and non-coordinated cyano groups though in the crystal structure of **1**, the deprotonated ligand lies in the highly symmetric structure, and only one type of C–N bonds is present. On the other hand, model M2 is too symmetric having only non-coordinated cyano groups in the imidazole rings, although in **2** one of the cyano groups is coordinated to nearby Cu_4I_4 motifs. Nevertheless, by combining the information obtained from the two models, we were able to interpret the most important peaks in the experimental spectra.

As the first interpretation, the experimentally observed unexpected shift to lower wave numbers, when the stretching frequencies of coordinated C–N groups were compared with the free dicyanoimidazole could be verified. It should be noted that the calculated frequencies were not scaled, and therefore the absolute values are somewhat overestimated. Nevertheless, the relative trends of the experimental spectra were well reproduced. The calculated ν(C–N) in free dicyanoimidazole were 2397 and 2384 cm^{-1}, which shifted to 2348 and 2344 cm^{-1} upon deprotonation. In model M1, the non-coordinated cyano groups gave stretching signals at 2371-2252 cm^{-1}, but the coordinated cyano groups showed clearly lower wave numbers, 2240-2230 cm^{-1}. However, this was not a result of the side-on coordination, but of the considerable redistribution of charge in the ligands. According to the QTAIM analysis, the coordinated nitrogen atoms gain electron density upon coordination, which interestingly affects the charge on the non-coordinated cyano groups as well.

When the experimental IR spectra for **1** and **2** are interpreted with the help of computational results, it can be seen, that the spectrum of **1**

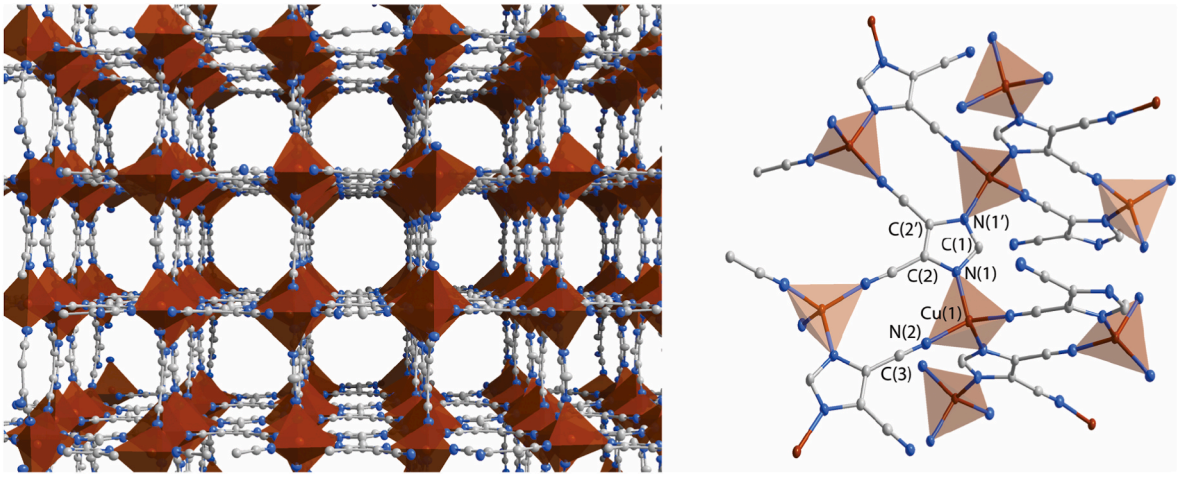

Fig. 1. $[Cu(4,5\text{-dicyanoimidazole})]_n(MeCN)_{0.5n}$ (1) The MeCN molecules in the pores are omitted. ($I4_122$, a = 9.2513(8) Å, b = 9.2513(8) Å, c = 22.279(2) Å).

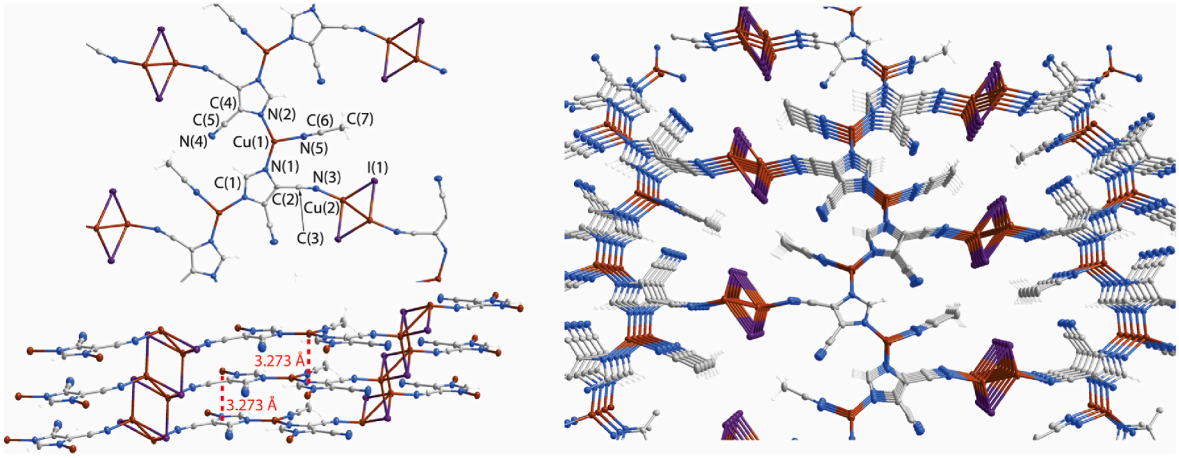

Fig. 2. [Cu(4,5-dicyanoimidazole)(MeCN)(CuI)]$_n$ (2) ($P2_1/c$, a = 4.3140(4) Å, b = 29.893(3), Å, c = 8.8458(8) Å, β = 100.540(2)°).

Table 1
Electrostatic potential (ESP) maps, and charges of the nitrogen atoms for the deprotonated (L(im)) and protonated (L(Him)) 4,5-dicyanoimidazole and MeCN L(ace) building blocks. The values in parenthesis represent charges in the solvent field of MeOH.

Molecule	ESP	q(N1)[a]	q(N2)[a]	q(N3)[b]	q(N4)[b]
L(im)		−1.251 (−1.269)	−1.251 (−1.269)	−1.382 (−1.390)	−1.382 (−1.390)
L(Him)		−1.325 (−1.319)	−1.190 (−1.217)	−1.229 (−1.287)	−1.246 (−1.314)
L(ace)				−1.324 (−1.402)	

[a] imidazole group.
[b] cyano groups.

shows peaks only for coordinated cyano groups (2233 cm^{-1}), but the spectrum of **2** shows both non-coordinated (2245 cm^{-1}) and coordinated (2233 cm^{-1}) C–N frequencies. This is consistent with the observed crystal structures. For further verification of the structure of **2**, the frequencies of model M2 were compared with those of free MeCN. Unfortunately, according to the simulations, the intensity of the C–N stretching frequency of MeCN is very low, and hence it cannot be seen in the experimental spectrum. In addition, the calculated ν(C–N) in free MeCN was 2408 cm^{-1}, and in the coordinated acetonitrile ligand in M2 2404 cm^{-1}. Therefore, the question whether the acetonitrile molecule is coordinated in **2** or not remains inconclusive according to IR spectrum.

2.2. Charge density of the building blocks

To explain the differences in the crystal formation, we calculated the relative charge distribution of the building blocks (dicyanoimidazole and acetonitrile) by using topological charge density analysis *via* Bader's Quantum Theory of Atoms in Molecules (QTAIM) method. Table 1 lists the nitrogen charges of each molecule with and without the solvent field of methanol (values in parentheses correspond to the molecules in MeOH). For 4,5-dicyanoimidazole, the effect of deprotonation was also studied. The Table includes the corresponding electrostatic potential (ESP) maps of the systems to visualize the differences.

Deprotonation of the imidazole ring modifies the originally rather uneven charge distribution of the 4,5-dicyanoimidazole into a balanced one, where the cyano nitrogens exhibit somewhat larger negative charge, and would be slightly more prone to attach to copper cations than the imidazole nitrogens. However, the difference is not large, and hence all nitrogens coordinate to copper ions in the structure of **1**. On the other hand, MeOH solution increases the negative nitrogen charge in MeCN more than in the dicyanoimidazoles, thus promoting its coordination to copper, when MeOH is present, as in the formation of **2**.

2.3. Nature of bonding in the crystals

We created more extended models for the crystalline state materials and studied the nature of the interactions in order to find the ones having major impact on the packing of the solid state structures. Fig. 3 shows the models, which were cut from the experimentally obtained crystal structures. The model for **1** included eight Cu atoms with the surrounding ligands, [Cu_8(4,5-dicyanoimidazole)$_{18}$], while the model for **2** consisted of six Cu atoms, ten dicyanoimidazole ligands, six acetonitriles, and two attached [Cu_4I_4] units, giving as the overall model [Cu_6(4,5-dicyanoimidazole)$_{10}$(MeCN)$_6$(CuI)$_8$]. Fig. 3 shows the bond critical points (BCPs) and the bond paths in the models according to the QTAIM analysis. The numbering scheme of the selected BCPs from the closest coordination sphere of copper ion is followed in Table 2, where the properties of the electron density at the BCPs are listed.

As can be seen from the larger electron density and the larger interaction energy at the Cu-NC bond critical point compared with the one forming with imidazole nitrogens, the cyano groups coordinate more strongly to copper ions in the structure of **1**. This is consistent with the charge distribution found in the free dicyanoimidazole ligand (Table 1), where the larger negative charge of the cyano nitrogen suggested stronger interaction with metal ions. However, the Cu-N_{im} also exhibits notable attractive interaction (−154 $kJmol^{-1}$), confirming that all nitrogens of the ligands have strong metal-ligand bonding with Cu. Interestingly, the coordination to copper has increased the electron density as well the strength of the C═N multiple bond of the cyano group compared with that of the free ligand. Typical of the metal-ligand bonding, the nature of all the Cu–N bonds is partially covalent, as can be seen from the |V|/G value, which falls between 1 and 2. The delocalization index (bond index) is around 0.5, again indicating that the Cu–N bonds are similar in nature. In compound **2**, the only difference is the reversed order in the values of the electron densities and interaction energies at the Cu-N_{im} and Cu-NC BCPs. Notably, the strength of interaction between copper ion and nitrogen of the MeCN molecule (BCP #2″) is about the same as that of the imidazole cyano groups in structure **1**. Because of the similar trends, the preferred N-coordination of copper ions to different types of ligands will be determined by the reaction conditions, such as the presence of methanol solvent in the case of structure **2**.

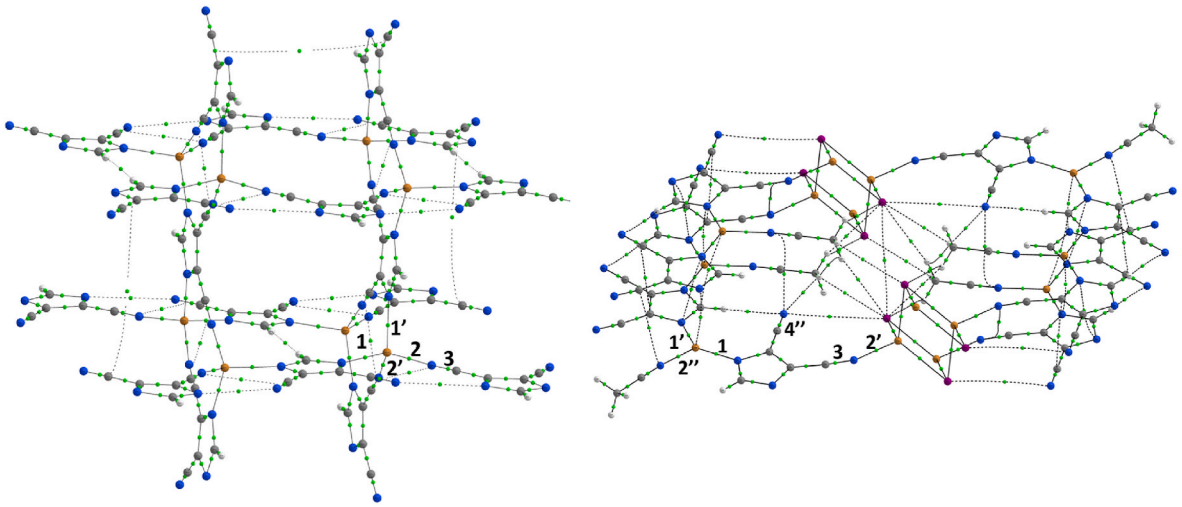

Fig. 3. Bond paths and bond critical points for computational models of **1** (left) and **2** (right). The color code is Cu = orange, N = blue, C = gray, H = white, I = purple. The numbering scheme of the BCPs is followed in Table 2.

Table 2
Properties of the electron density at the selected bond critical points (see Fig. 3) of crystal structures of **1** and **2**, and the free ligands L(im) and L(ace). ρ = electron density at the BCP, |V|/G = ratio between potential energy density and kinetic energy density, DI(A,B) = delocalization index between atoms A and B, E_{INT} = interaction energy.

BCP#	Type	ρ (eÅ^{-3})	|V|/G	DI(A,B)	E_{INT} (kJmol^{-1})
[Cu_8(4,5-dicyanoimidazole)$_{18}$] (1)					
1	Cu-N_{im}	0.506	1.15	0.46	−153
1′	Cu-N_{im}	0.509	1.15	0.46	−154
2	Cu-NC	0.607	1.18	0.56	−212
2′	Cu-NC	0.610	1.18	0.56	−213
3	C–N	3.179	1.83	2.01	−2382
[Cu_6(4,5-dicyanoimidazole)$_{10}$(MeCN)$_6$(CuI)$_8$] (2)					
1	Cu-N_{im}	0.642	1.22	0.57	−213
1′	Cu-N_{im}	0.684	1.23	0.58	−236
2′	Cu-NC[a]	0.548	1.16	0.49	−180
2″	Cu-NC(ace)	0.571	1.17	0.51	−194
3	C–N	3.098	1.87	2.06	−2271
4″	C–N[b]	3.241	1.81	2.13	−2461
4,5-dicyanoimidazole (L(im))					
3	C–N	3.080	1.88	2.19	−2238
3′	C–N	3.079	1.88	2.19	−2237
Me(CN) (L(ace))					
3	C–N	3.112	1.85	2.28	−2307

[a] interaction to Cu_4I_4 motif.
[b] non-coordinated cyano group.

3. Experimental

3.1. Materials and methods

Commercially available reagents CuI (98%, Sigma-Aldrich) and 1,5–dicyanoimidazole (99%, Aldrich) were used without purification. The organic solvents were dried using molecular sieves. Infrared spectra were measured from KBr pellets using Bruker Vertex 70 Fourier transform infrared spectrophotometer in the range of 4000–400 cm^{-1}. The elemental analysis was performed on varioMICRO V1.7.

3.2. Crystal structure determination

The crystals of **1** and **2** were immersed in cryo-oil, mounted in a Nylon loop, and measured at a temperature of 150 K. The X-ray diffraction data were collected on a Bruker Kappa Apex II diffractometer using Mo K_α radiation (λ = 0.71073 Å). The APEX2 [32] program package was used for cell refinements and data reductions. The structures were solved by direct methods using the SHELXS-2018 [33] program with the WinGX [34] graphical user interface. A numerical absorption correction (SADABS) [35] was applied to all data. Structural refinements were carried out using SHELXL-2018 [33].

The N–H hydrogen atoms were located from the difference Fourier map and constrained to ride on their parent atoms, with U_{iso} = 1.2 U_{eq} (parent atom). All other hydrogen atoms were positioned geometrically and constrained to ride on their parent atoms, with C–H = 0.95–0.98 Å and U_{iso} = 1.2–1.5 U_{eq} (parent atom). The crystallographic details are summarized in Table S1.

3.3. Computational details

All calculations were performed by applying Gaussian 09 software package [36]. The optimized geometry and simulated infrared spectra with no scaling for small molecular models of the structures were obtained by PBE0 functional [37] with 6-31G(d) basis set for C, N, and H atoms and def2-TZVPPD basis set [38] for Cu and I atoms.

To obtain the electronic properties of the solid state structure of **2**, and to compare those with the structure of **1**, we performed topological charge density analysis with the QTAIM (Quantum Theory of Atoms in Molecules) [39] method, which allowed us to access the nature of the bonding *via* calculating different properties of the electron density at the bond critical points (BCPs). The analysis was done with the AIMALL program [40] using the wavefunction obtained from the single point DFT calculations of extended models cut directly from the crystal structure and used without optimization.

3.4. Synthesis of [Cu(4,5-dicyanoimidazole)]$_n$(MeCN)$_{0.5n}$ (1)

CuI (32.3 mg, 0.169 mmol) was dissolved in MeCN (1.0 ml). 4,5-dicyanoimidazole (20.2 mg, 0.171 mmol) was dissolved in MeCN (0.5 ml). The solutions were combined. After a few weeks, colorless crystals at +4 °C were formed. Yield 7.3 mg. IR (KBr): ν(C–N) 2233 cm^{-1}. Calc. for $C_6H_{2,5}N_{4,5}Cu$ C% 35.83; H% 1.25; N% 31.33. Found. C% 36.99; H% 1.73; N% 30.74.

3.5. Synthesis of [Cu(4,5-dicyanoimidazole)(MeCN)(CuI)]$_n$ (2)

CuI (32.2 mg, 0.169 mmol) was dissolved in MeCN (1.0 ml). 4,5-dicyanoimidazole (19.8 mg, 0.168 mmol) was dissolved in MeOH (0.5 ml). The solutions were combined. After a few weeks, yellow crystals at +4 °C were formed. Yield 10.6 mg. IR (KBr): ν(C–N) 2233, 2245 cm^{-1}. Calc. for $C_7H_4N_5ICu_2$ C% 20.40; H% 0.98; N% 16.99. Found.

C% 21.24; H% 1.06; N% 17.01.

4. Conclusions

In this paper, we present one-pot reactions of the same reactants 4,5-dicyanoimidazole and CuI in different solvents. The presence of methanol solvent in the crystallization process was found to affect the final crystal structure of the product. In pure MeCN, crystallization yields a known 3D MOF structure **1**. However, if the crystallization is done in the mixture of acetonitrile and methanol, the latter promotes the coordination of MeCN to copper ions, and a new polymeric chain structure **2** is formed. Computational studies revealed that the explanation for the better coordination of MeCN lies in the increasing negative charge at the nitrogen end of the molecule from the original non-solvent value of −1.324 to −1.402 in the methanol solvent field. Therefore, in MeCN/MeOH solvent mixture the acetonitrile molecules bind to copper and form the coordination polymer structure **2**, while in the MOF structure **1** the MeCN solvent is included in the pores only with weak hydrogen-bonding interactions. According to the QTAIM analysis, the nature of the metal coordination is similar for all nitrogen donors of the ligands, including MeCN. The Cu–N bonds are typical, rather strong metal-ligand bonds exhibiting interaction energies around −150 to −230 $kJmol^{-1}$, some electron sharing, and delocalization indices around 0.5. Therefore, the preferred coordination modes will depend on subtle changes in the reaction conditions when the compounds crystallize.

Author statement

All authors have seen and approved the final version of the manuscript being submitted. We warrant that the article is the authors' original work, hasn't received prior publication and isn't under consideration for publication elsewhere.

Declaration of competing interest

The authors declare that they have no known competing financial interests or personal relationships that could have appeared to influence the work reported in this paper.

Acknowledgements

We acknowledge grants of computer capacity from the Finnish Grid and Cloud Infrastructure (persistent identifier urn:nbn:fi:research-infras-2016072533).

Appendix A. Supplementary data

Supplementary data to this article can be found online at https://doi.org/10.1016/j.solidstatesciences.2022.106885.

References

[1] Z. Han, W. Shi, P. Cheng, Synthetic strategies for chiral metal-organic frameworks Chin, Chem. Lett. 29 (2017) 819–822, https://doi.org/10.1016/j.cclet.2017.09.050.
[2] S. Yuan, L. Feng, K. Wang, J. Pang, M. Bosch, C. Lollar, Y. Sun, J. Qin, X. Yang, P. Zhang, Q. Wang, L. Zou, Y. Zhang, L. Zhang, Y. Fang, J. Lim, H.-K. Zhou, Stable metal–organic frameworks: design, synthesis, and applications, Adv. Mater. 30 (2018), https://doi.org/10.1002/adma.201704303, 1704303- 170.
[3] R. Seetharaj, P.V. Vandana, P. Arya, S. Mathew, Dependence of solvents, pH, molar ratio and temperature in tuning metal organic framework architecture Arabian, J. Chem. 12 (2019) 295–315, https://doi.org/10.1016/j.arabjc.2016.01.003.
[4] N. Stock, S. Biswas, Synthesis of metal-organic frameworks (MOFs): routes to various MOF topologies, morphologies, and composites, Chem. Rev. 112 (2012) 933–969, https://doi.org/10.1021/cr200304e.
[5] H. Zhu, D. Liu, The synthetic strategies of metal-organic framework membranes, films and 2D MOFs and their applications in devices, J. Mater. Chem. 7 (2019) 21004–21035, https://doi.org/10.1039/c9ta05383b.
[6] G. Xu, P. Nie, H. Dou, B. Ding, L. Li, X. Zhang, Exploring metal organic frameworks for energy storage in batteries and supercapacitors Mater, Today Off. 20 (2017) 191–209, https://doi.org/10.1016/j.mattod.2016.10.003.
[7] A.E. Baumann, D.A. Burns, B. Liu, V.S. Thoi, Metal-organic framework functionalization and design strategies for advanced electrochemical energy storage devices Commun, Inside Chem. 2 (2019) 86, https://doi.org/10.1038/s42004-019-0184-6.
[8] J. Ren, H.W. Langmi, B.C. North, M. Mathe, Review on processing of metal–organic framework (MOF) materials towards system integration for hydrogen storage Int, J. Energy Res. 39 (2015) 607–620, https://doi.org/10.1002/er.3255.
[9] Y. Xue, S. Zheng, H. Xue, H. Pang, Metal–organic framework composites and their electrochemical applications, J. Mater. Chem. 7 (2019) 7301–7327, https://doi.org/10.1039/C8TA12178H.
[10] Y. Liu, X.-Y. Xie, C. Cheng, Z.-S. Shao, H.-S. Wang, Strategies to fabricate metal–organic framework (MOF)-based luminescent sensing platforms, J. Mater. Chem. C 7 (2019) 10743–10763, https://doi.org/10.1039/C9TC03208H.
[11] Q. Wang, D. Astruc, State of the art and prospects in Metal−Organic framework (MOF)-Based and MOF-derived nanocatalysis, Chem. Rev. 120 (2020) 1438–1511, https://doi.org/10.1021/acs.chemrev.9b00223.
[12] B. Sieklucka, R. Podgajny, T. Korzeniak, B. Nowicka, D. Pinkowicz, M. Kozieł, A decade of octacyanides in polynuclear molecular materials, Eur. J. Inorg. Chem. (2011) 305–326, https://doi.org/10.1002/ejic.201001055.
[13] G.M. Espallargas, E. Coronado, Magnetic functionalities in MOFs: from the framework to the pore, Chem. Soc. Rev. 47 (2018) 533–557, https://doi.org/10.1039/c7cs00653e.
[14] Z.-H. Yan, D. Li, X.-B. Yin, Review for chiral-at-metal complexes and metal-organic framework enantiomorphs, Sci. Bull. 62 (19) (2017) 1344–1354, https://doi.org/10.1016/j.scib.2017.09.013.
[15] W. Bury, D. Fairen-Jimenez, M.B. Lalonde, R.Q. Snurr, O.K. Farha, J.T. Hupp, Control over catenation in pillared paddlewheel Metal−Organic framework materials via solvent-assisted linker exchange chem, Mater 25 (2013) 739–744, https://doi.org/10.1021/cm303749m|.
[16] O.K. Farha, C.D. Malliakas, M.G. Kanatzidis, J.T. Hupp, Control over catenation in metal-organic frameworks via rational design of the organic building block, J. Am. Chem. Soc. 132 (2010) 950–952, https://doi.org/10.1021/ja909519e.
[17] L. Zhang, F. Liand, L. Luo, Preparation methods of metal organic frameworks and their capture of CO2, IOP Conf. Ser. Earth Environ. Sci. 108 (2018), https://doi.org/10.1088/1755-1315/108/4/042104, 042104.
[18] S.R. Jambovane, S.K. Nune, R.T. Kelly, B.P. McGrail, Z. Wang, M.I. Nandasiri, S. Katipamula, C. Trader, H.T. Schaef, Continuous, one-pot synthesis and post-synthetic modification of NanoMOFs using droplet nanoreactors, Sci. Rep. 6 (2016) 36657, https://doi.org/10.1038/srep36657.
[19] F. Israra, D.K. Kimb, Y. Kima, W. Chuna, Scope of various solvents and their effects on solvothermal synthesis of Ni-BTC Quim, Nova 39 (6) (2016) 669–675, https://doi.org/10.5935/0100-4042.20160068.
[20] L. Luo, G.-C. Lv, P. Wang, Q. Liu, K. Chen, W.-Y. Sun, pH-Dependent cobalt(ii) frameworks with mixed 3,3′,5,5′-tetra(1*H*-imidazole-1-yl)-1,1′-biphenyl and 1,3,5-benzenetricarboxylate ligands: synthesis, structure and sorption property, CrystEngComm 15 (2013) 9537–9543, https://doi.org/10.1039/C3CE41056K.
[21] W. Xuan, R. Ramachandran, C. Zhao, F. Wang, Influence of synthesis temperature on cobalt metal-organic framework(Co-MOF) formation and its electrochemical performance towards supercapacitor electrodes, J. Solid State Electrochem. 22 (2018) 3873–3881, https://doi.org/10.1007/s10008-018-4096-7.
[22] P. Nian, H. Liu, X. Zhang, Bottom-up synthesis of 2D Co-based metal–organic framework nanosheets by an ammonia-assisted strategy for tuning the crystal morphology, CrystEngComm 21 (2019) 3199–3208, https://doi.org/10.1039/C9CE00259F.
[23] C.R. Marshall, S.A. Staudhammer, C.K. Brozek, Size control over metal–organic framework porous nanocrystals, Chem. Sci. 10 (2019) 9396–9408, https://doi.org/10.1039/C9SC03802G.
[24] X.-Z. Wang, M.-Y. Sun, J. Zheng, D. Luo, L. Qi, X.-P. Zhou, D. Li, Coordination-driven self-assembly of M10L8 metal–organic bi-capped square antiprisms with adaptable cavities, Dalton Trans. 48 (2019) 17713–17717, https://doi.org/10.1039/c9dt04368c.
[25] J. Kim, S.-T. Yang, S.B. Choi, J. Sim, J. Kim, W.-S. Ahn, Control of catenation in CuTATB-n metal–organic frameworks by sonochemical synthesis and its effect on CO2 adsorption, J. Mater. Chem. 21 (2011) 3070–3076, https://doi.org/10.1039/C0JM03318A.
[26] B. Zhang, J. Zhang, C. Liu, X. Sang, L. Peng, X. Ma, T. Wu, B. Han, G. Yang, Solvent determines the formation and properties of metal-organic framework, RSC Adv. 5 (2015) 37691–37696, https://doi.org/10.1039/C5RA02440D.
[27] J. Hungerford, K.S. Walton, Room-temperature synthesis of Metal−Organic framework isomers in the tetragonal and kagome crystal structure inorg, Inside Chem. 58 (2019) 7690–7697, https://doi.org/10.1021/acs.inorgchem.8b03202.
[28] T.-P. Hu, X.-X. Wang, B.-H. Zheng, X.-Q. Wang, X.-N. Hao, J.-F. Liu, Assembly of a 3D chiral Cu(I) metal–organic framework based on 4,5-dicyanoimidazole: CD spectrum, luminescence and selective gas adsorption Inorg, Chem. Comm. 68 (2016) 17–20, https://doi.org/10.1016/j.inoche.2016.03.024.
[29] N. Zhao, P. Li, X. Mu, C. Liu, F. Sun, G. Zhu, Facile synthesis of an ultra-stable metal-organic framework with excellent acid and base resistance, Faraday Discuss 201 (2017) 63–70, https://doi.org/10.1039/C7FD00017K.
[30] N. Zhao, L. Yang, B. Xie, J. Han, Q. Pan, X. Li, M. Liu, Y. Wang, X. Wang, G. Zhu, Organic amines as templates: pore imprints with exactly matching sizes in a series of metal–organic frameworks, Chem. Commun. 54 (2018) 11264–11267, https://doi.org/10.1039/C8CC05404E.

[31] K.D. Shimizu, J. Rebek Jr., A rigid trans-spanning dinitrile ligand, Proc. Natl. Acad. Sci. Unit. States Am. 93 (1996) 4257–4260.
[32] APEX2 - Software Suite for Crystallographic Programs, Bruker AXS, Inc., Madison, WI, USA, 2010.
[33] G.M. Sheldrick, Crystal structure refinement with SHELXL, Acta Crystallogr. C: Struct. Chem. 71 (2015) 3–8, https://doi.org/10.1107/S2053229614024218.
[34] L.J. Farrugia, WinGX and ORTEP for windows: an update, J. Appl. Crystallogr. 45 (2012) 849–854, https://doi.org/10.1107/S0021889812029111.
[35] G.M. Sheldrick, SADABS-2008/1 - Bruker AXS Area Detector Scaling and Absorption Correction, Bruker AXS, Madison, Wisconsin, USA, 2008.
[36] M.J. Frisch, G.W. Trucks, H.B. Schlegel, G.E. Scuseria, M.A. Robb, J.R. Cheeseman, G. Scalmani, V. Barone, B. Mennucci, G.A. Petersson, H. Nakatsuji, M. Caricato, X. Li, H.P. Hratchian, A.F. Izmaylov, J. Bloino, G. Zheng, J.L. Sonnenberg, M. Hada, M. Ehara, K. Toyota, R. Fukuda, J. Hasegawa, M. Ishida, T. Nakajima, Y. Honda, O. Kitao, H. Nakai, T. Vreven, J.A. Montgomery Jr., J.E. Peralta, F. Ogliaro, M. Bearpark, J.J. Heyd, E. Brothers, K.N. Kudin, V.N. Staroverov, R. Kobayashi, J. Normand, K. Raghavachari, A. Rendell, J.C. Burant, S.S. Iyengar, J. Tomasi, M. Cossi, N. Rega, J.M. Millam, M. Klene, J.E. Knox, J.B. Cross, V. Bakken, C. Adamo, J. Jaramillo, R. Gomperts, R.E. Stratmann, O. Yazyev, A.J. Austin, R. Cammi, C. Pomelli, J.W. Ochterski, R.L. Martin, K. Morokuma, V.G. Zakrzewski, G.A. Voth, P. Salvador, J.J. Dannenberg, S. Dapprich, A.D. Daniels, Ö. Farkas, J. B. Foresman, J.V. Ortiz, J. Cioslowski, D.J. Fox, Gaussian 09, Revision C.01D, Gaussian, Inc., Wallingford CT, 2009.
[37] J.P. Perdew, M. Ernzerhof, K. Burke, Rationale for mixing exact exchange with density functional approximations, J. Chem. Phys. 105 (1996) 9982–9985, https://doi.org/10.1063/1.472933.
[38] D. Rappoport, F. Furche, Property-optimized Gaussian basis sets for molecular response calculations, J. Chem. Phys. 133 (2010) 134105, https://doi.org/10.1063/1.3484283.
[39] R.F.W. Bader, Atoms in Molecules: A Quantum Theory, Oxford University Press, Oxford, 1990.
[40] T.A. Keith, AIMAll (Version 19.02.13), TK Gristmill Software; aim.tkgristmill.com, Overland Park, KS, USA, 2019.